

# <sup>1</sup> 3DQLayers: Volumetric Layer Based Analysis for Quantitative Renal MRI

<sup>3</sup> Alexander J Daniel  and Susan T Francis  

<sup>4</sup> 1 Sir Peter Mansfield Imaging Centre, University of Nottingham, Nottingham, United Kingdom 2 NIHR  
<sup>5</sup> Nottingham Biomedical Research Centre, Nottingham University Hospitals NHS Trust and the University  
<sup>6</sup> of Nottingham, Nottingham, United Kingdom ¶ Corresponding author

DOI: [10.xxxxxx/draft](https://doi.org/10.xxxxxx/draft)

## Software

- [Review](#) 
- [Repository](#) 
- [Archive](#) 

---

Editor: [Open Journals](#) 

Reviewers:

- [@openjournals](#)

Submitted: 01 January 1970

Published: unpublished

## License

Authors of papers retain copyright and release the work under a Creative Commons Attribution 4.0 International License ([CC BY 4.0](#)).

## <sup>7</sup> Summary

<sup>8</sup> Quantitative Magnetic Resonance Imaging (qMRI) provides informative measurements of <sup>9</sup> structure and function of an organ where each volumetric pixel (voxel) provides a measure <sup>10</sup> of the physical properties of the underlying tissue. Traditionally, analysis of MR images <sup>11</sup> is performed by first segmenting the organ and its constituent tissue types, which for the <sup>12</sup> kidneys involves separating them into the cortex and medulla, before calculating the average <sup>13</sup> measurement within each voxel. The process of segmenting renal tissue types is typically <sup>14</sup> manual, making it time consuming and prone to inaccuracies.

<sup>15</sup> An alternative to voxel-based analysis in MRI is the layer model which divides the organ into <sup>16</sup> ordered surfaces. For the kidney, this involves generating layers based on the distance of each <sup>17</sup> voxel between the outer and inner surface of the kidney. From this, the gradient of change in <sup>18</sup> qMRI measures between the cortex and medulla of the kidney can be computed to evaluate <sup>19</sup> pathological and physiological aspects of the kidney. Here, 3DQLayers an open-source Python <sup>20</sup> software package to automatically define and interrogate 3D renal layers is presented.

## <sup>21</sup> Statement of need

### <sup>22</sup> Background

<sup>23</sup> The kidneys are structurally and functionally complex organs in the abdomen responsible for <sup>24</sup> the removal of waste products and excess fluid from the blood to produce urine ([Lote, 2012](#)). <sup>25</sup> Each kidney is separated into the cortex which forms the outer layer of the kidney and the <sup>26</sup> medulla in the inner part which is arranged in a series of small pyramids ([Hall, 2015](#)), as shown <sup>27</sup> in [Figure 1](#). The kidney maintains homeostasis through filtration, reabsorption, secretion, and <sup>28</sup> maintenance of the cortico-medullary gradient (CMG), meaning a method to assess changes in <sup>29</sup> physiology from the cortex to the medulla is a key.

<sup>30</sup> Quantitative MRI (qMRI) goes beyond conventional MRI which primarily assesses signal <sup>31</sup> intensity in a voxel in arbitrary units, by instead providing voxel-wise measurements with <sup>32</sup> numerical significance, in physical units, based on the tissues underlying properties. For <sup>33</sup> example, qMRI of relaxation times with parameters which carry information about the local <sup>34</sup> microstructural, or those of how readily water can diffuse through the tissue and the rate at <sup>35</sup> which blood perfuses the tissue. To interpret quantitative images, regions of interest (ROIs) <sup>36</sup> for the renal cortex and medulla are defined in the tissue and statistical analysis performed <sup>37</sup> on the voxels within each. Segmenting such ROIs manually is time consuming, and prone to <sup>38</sup> intra- and inter-reader variation.

<sup>39</sup> The group of Pruijm proposed an alternative to tissue ROI based analysis termed the Twelve <sup>40</sup> Layer Concentric Object (TLCO) method ([Li et al., 2020](#); [Milani et al., 2017](#); [Piskunowicz](#)

et al., 2015) where users delineate the inner and outer boundaries of the kidney to generate twelve equidistant layers between the renal pelvis and the surface of the kidney. The outer layers represent the cortex and the inner layers the medulla, the gradient across central layers (the CMG) can also be computed. Since this layer-based analysis only requires segmenting the boundaries of the kidney rather than the cortex and medulla within it is quicker and more repeatable. An analogy to this is the development of layer-based analysis tools applied in the brain for neuroimaging including BrainVoyager (Goebel, 2012), CBSTools/Nighres (Bazin et al., 2014; J. Huntenburg et al., 2017; J. M. Huntenburg et al., 2018), FreeSurfer (Fischl, 2012), and FSL (Jenkinson et al., 2012).

However, the TLCO software is closed source and has some limitations. It requires manual delineation of the outside and inside surfaces of the kidney, divides the kidney into the same number of layers irrespective of the size of the kidney, and can only be performed on a single slice cutting through the kidneys on their longest axis (coronal-oblique) which is not always desirable (Bane et al., 2020). Due to the spatial distribution of kidney pathology, researchers prefer to acquire multi-slice images for full 3D coverage of the kidney to increase the number of voxels sampled and gain a better understanding of the heterogeneity of the kidney. An automated-TLCO method has been proposed (Ishikawa et al., 2022), however this work highlights difficulties analysing small kidneys due to the limited layer thickness and is only applied to water images from a Dixon protocol.

The motivation of 3DQLayers was to address these limitations of TLCO to provide an open-source Python package to automatically define 3D, multi-slice, layers in the kidney of known thickness for quantitative-depth based analysis of kidney MRI data, enabling its use in large studies.

## Methods

3DQLayers is an open-source Python package building on the ideas within TLCO, with the fundamental difference that the layers are defined based a voxels' distance from the surface of the kidney in millimetres rather than the proportion of the kidney for 3D analysis. As such, the input to 3DQLayers is a whole kidney mask, which can be automatically generated from a structural image (e.g. using a U-net applied to T<sub>2</sub>-weighted images (Daniel et al., 2021; Daniel, 2024)).

The pipeline for defining the layers from the whole kidney mask is outlined in Figure 2. Pre-processing steps fill in holes in the kidney mask caused by cysts as the surface of a cyst is not characteristic of the surface of the kidney. Next the voxel-based representation of the ROI is converted to a smoothed mesh-based representation of the kidneys, the distance from the centre of each voxel to the surface of the mesh is then calculated to produce a depth map (Dawson-Haggerty, 2023). Tissue adjacent to the renal pelvis that is not representative of the medulla is then excluded from layer-based analysis. This is achieved by automatically segmenting the pelvis then calculating the distance from each voxel to the pelvis using the method described as above. Voxels closer than a specified threshold, typically 10 mm, are then excluded from the depth map. Finally, a layer image is generated by quantising the depth map to a desired layer thickness, typically 1 mm.

The layer image and quantitative images are resampled to the same spatial resolution using NiBabel (Brett et al., 2023), to allow each layer to be used as an ROI to interrogate each qMRI image with statistical measures (e.g. median, standard deviation and kurtosis) across the depth of the kidney. The gradient of the central layers can be calculated to estimate the CMG in qMRI metrics. Additionally, if cortex and medulla ROI are available the distribution of tissue types across layer depth can be explored. The left and right kidney can be analysed separately or combined. As the layers are generated from a structural image rather than the quantitative map, using 3DQLayers stipulates no requirements on quantitative map acquisition, unlike TLCO.

91 An object-oriented interface is provided to allow end users to simply generate layers and apply  
 92 these to quantitative MR images. Documentation is provided to guide users through installation  
 93 via PyPI, conda or from source code on GitHub and includes tutorials and an API reference.  
 94 An automated test suite with high coverage provides users with confidence in the stability of  
 95 3DQLayers and that there will be no unexpected changes to results unless highlighted in the  
 96 change-log.

## 97 Usage Examples

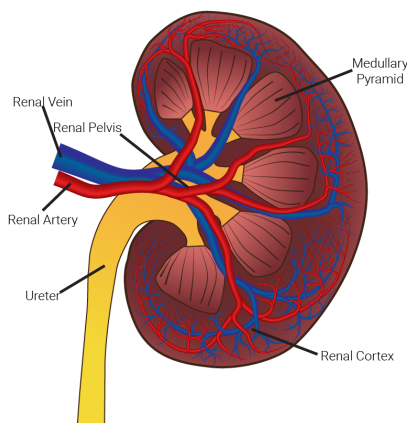
98 **Figure 3** shows 3DQLayers being used to measure different gradients of  $R_2^*$  in a healthy volunteer  
 99 with normal and patient with impaired renal function (an estimated glomerular filtration rate  
 100 (eGFR) of above 90 ml/min/1.73m<sup>2</sup> measured from blood samples is considered in the healthy  
 101 range (Stevens et al., 2006)). This replicates results shown using TLCO of a lower gradient in  
 102 patients, however 3DQLayers controls for kidney size resulting in the gradient being measured in  
 103 quantitative units of Hz/mm rather than Hz/layer as in TLCO, thus increasing generalisability.

104 **Figure 4** shows how 3DQLayers can be used in combination with cortex and medulla tissue  
 105 ROIs to analyse the distribution of voxel counts of each tissue as a function of layer depth of  
 106 the kidney. From this, average cortical thickness can be defined as the depth at which the  
 107 voxel distribution crosses from cortex to medulla. Cortical thickness has been hypothesised as  
 108 a potential biomarker of renal disease (Yamashita et al., 2015). Here cortex and medulla ROIs  
 109 are initially generated using a Gaussian mixture model to segment a T<sub>1</sub>-weighted structural  
 110 image followed by manual ROI correction.

111 3DQLayers can also be used to analyse ex-vivo kidneys outside the body. **Figure 5** shows  
 112 example quantitative maps acquired from a kidney removed for transplant but subsequently  
 113 deemed unsuitable and the associated layer profiles. **Figure 6** compares the results of tissue ROI  
 114 based analysis and layer-based analysis in fifteen transplant kidneys. A significant correlation  
 115 between outer layers and the cortex, and inner layers and the medulla was shown across all  
 116 quantitative mapping techniques and a significant correlation between cortico-medullary ratio  
 117 and layer gradient was shown for T<sub>1</sub>, T<sub>2</sub>, T<sub>2</sub><sup>\*</sup> and Magnetisation Transfer Ratio (MTR)  
 118 mapping.

## 119 Figures

a.



b.

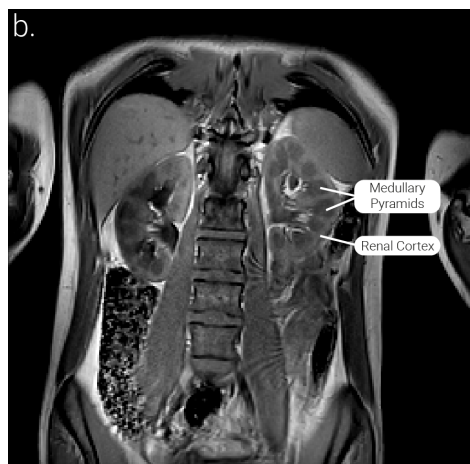


**Figure 1:** a) A schematic of the kidneys showing the renal cortex and medullary pyramids. b) A T<sub>1</sub>-weighted structural MR image of the abdomen showing the kidneys with the renal cortex appearing as a light band on the outer edge of the kidney and the medullary pyramids as darker patches on the inner portion of the kidneys.

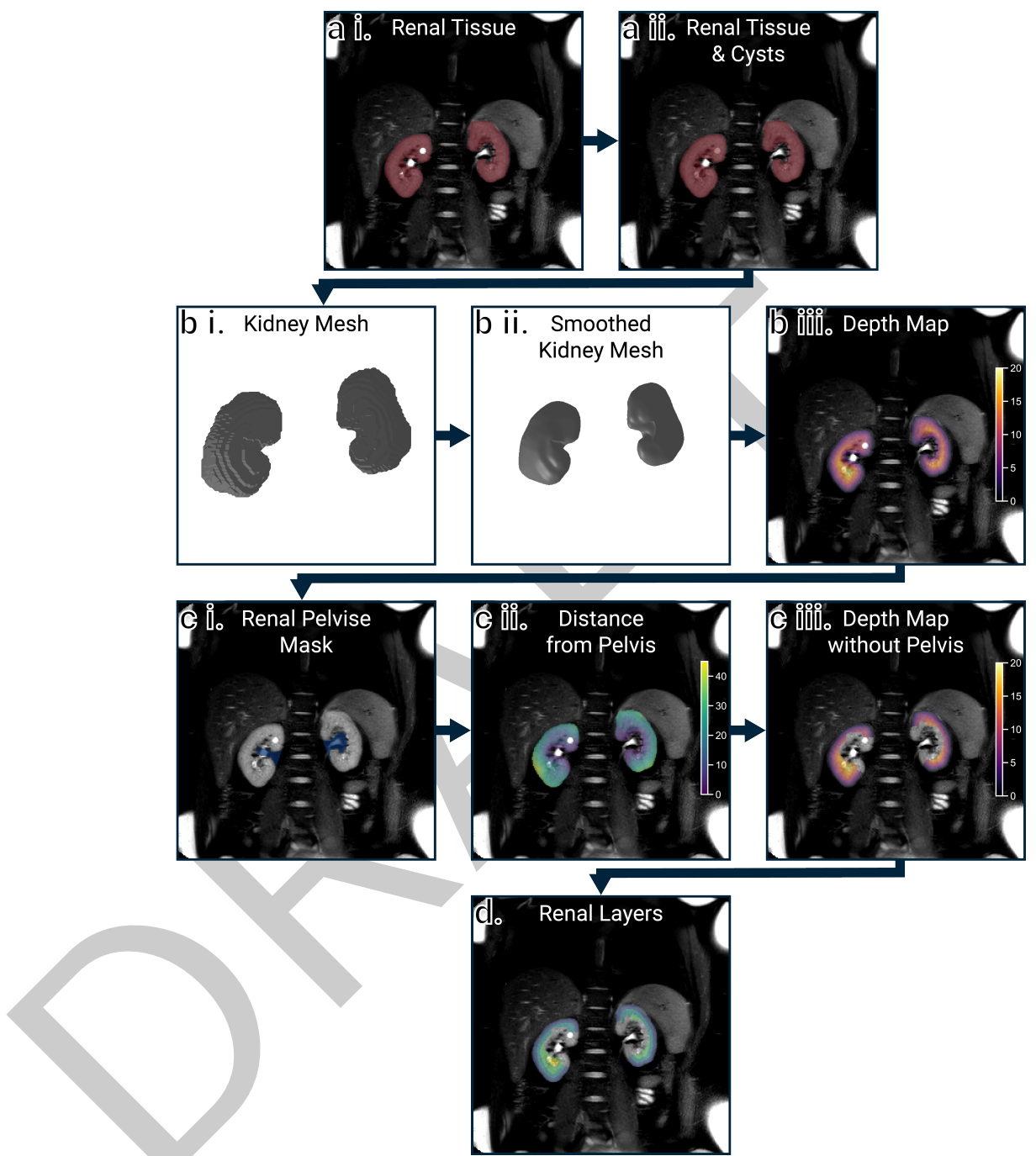


**Figure 2:** The mask automatically computed using a U-net from the T<sub>2</sub>-weighted structural MR image (a i) has any cysts filled (a ii) and is converted into a smooth mesh representing the renal surface (b i and ii). The distance (in mm) of each voxel to the surface of the mesh is then calculated to generate a depth map (b iii). The renal pelvis is segmented (c i) and any tissue within 10 mm (c ii) of the pelvis is excluded from the depth map (c iii). The tissue is then grouped into layers of a desired thickness, here shown as 5 mm renal layers for illustrative purposes (d).

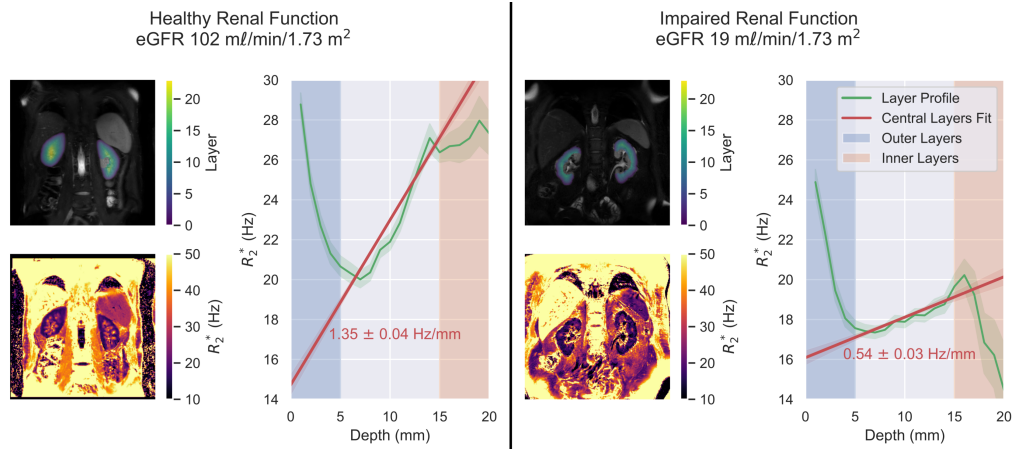


**Figure 3:** Layers,  $R_2^*$  maps, layer profiles, and central layer gradients for both left and right kidneys combined measured using 3DQLayers. Examples are shown for a subject with normal renal function and a patient with impaired renal function. Shading around profiles shows the 95% confidence interval within each layer.

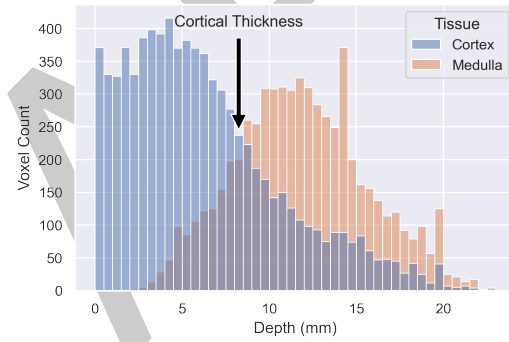


**Figure 4:** Exploring the distribution of tissue types through the kidney to measure cortical thickness.

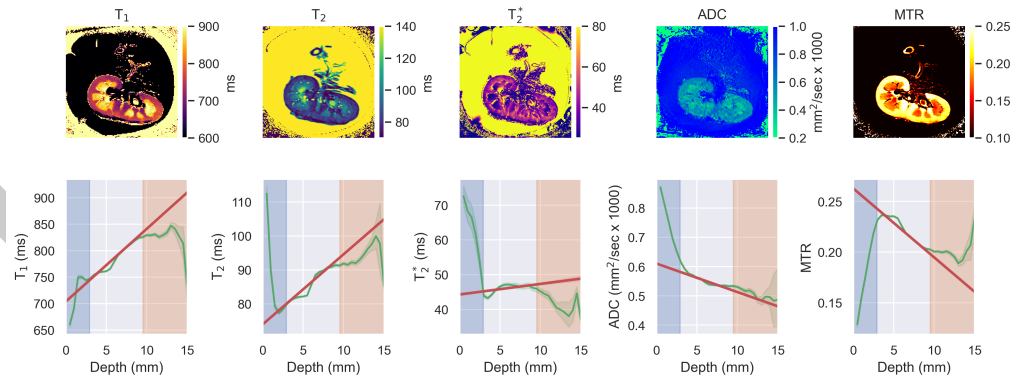


**Figure 5:** Example quantitative maps and associated layer profiles when 3DQLayers is applied to ex-vivo transplant kidneys. Uncertainty shading shows the 95% confidence interval of each layer.

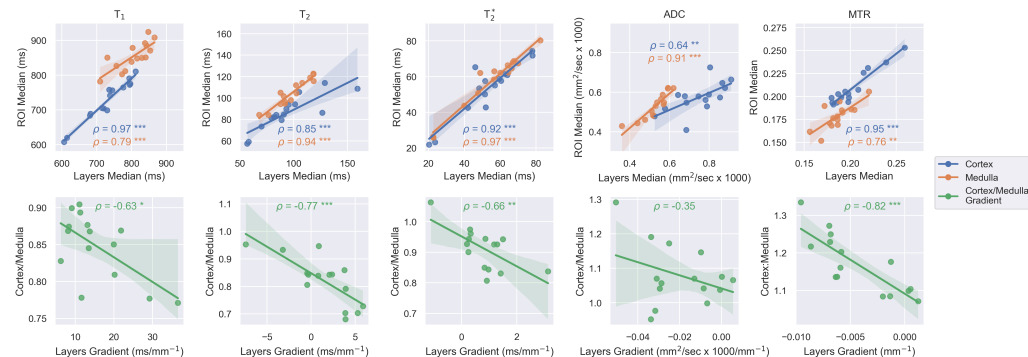


**Figure 6:** Agreement between tissue ROI-based measures and analogous layer-based measures shown for fifteen ex-vivo transplant kidneys for each qMRI with the Pearson's correlation coefficient ( $\rho$ ). \* represents a  $p$ -value between 0.05 and 0.1, \*\* between 0.01 and 0.001, and \*\*\*  $< 0.001$ . a) Plots the median within each tissue ROI (cortex or medulla semi-automatically defined) against the equivalent layers (outer layers and inner layers respectively as highlighted in Figure 5)b) Shows the cortico-medullary ratio (calculated by dividing the median within the cortex ROI by the median within the medullary ROI) against central layer gradient profiles calculated using 3DQLayers.

## 120 Acknowledgements

121 We acknowledge the funding support of Kidney Research UK (KS\_RP\_002\_20210111),  
 122 Medical Research Council (MR/R02264X/1), NIHR (NIHR128494), and NIHR Nottingham  
 123 Biomedical Research Centre during the genesis of this project.

## 124 References

- 125 Bane, O., Mendichovszky, I. A., Milani, B., Dekkers, I. A., Deux, J.-F., Eckerbom, P., Grenier,  
 126 N., Hall, M. E., Inoue, T., Laustsen, C., Lerman, L. O., Liu, C., Morrell, G., Pedersen,  
 127 M., Pruijm, M., Sadowski, E. A., Seeliger, E., Sharma, K., Thoeny, H., ... Prasad, P. V.  
 128 (2020). Consensus-based technical recommendations for clinical translation of renal BOLD  
 129 MRI. *Magnetic Resonance Materials in Physics, Biology and Medicine*, 33(1), 199–215.  
<https://doi.org/10.1007/s10334-019-00802-x>
- 130 Bazin, P.-L., Weiss, M., Dinse, J., Schäfer, A., Trampel, R., & Turner, R. (2014). A  
 131 computational framework for ultra-high resolution cortical segmentation at 7 Tesla.  
 132 *NeuroImage*, 93, 201–209. <https://doi.org/10.1016/j.neuroimage.2013.03.077>
- 133 Brett, M., Markiewicz, C. J., Hanke, M., Côté, M.-A., Cipollini, B., McCarthy, P., Cheng, C.  
 134 P., Halchenko, Y. O., Cottaar, M., Ghosh, S., Larson, E., Wassermann, D., Gerhard, S.,  
 135 Lee, G. R., Kastman, E., Rokem, A., Madison, C., Morency, F. C., Moloney, B., ... freec84.  
 136 (2023). NiBabel (Version 5.1.0). Zenodo. <https://doi.org/10.5281/zenodo.591597>
- 137 Daniel, A. J. (2024). *Renal Segmentor* (Version 1.3.9). <https://doi.org/10.5281/zenodo.4068850>
- 138 Daniel, A. J., Buchanan, C. E., Allcock, T., Scerri, D., Cox, E. F., Prestwich, B. L., & Francis,  
 139 S. T. (2021). Automated renal segmentation in healthy and chronic kidney disease subjects  
 140 using a convolutional neural network. *Magnetic Resonance in Medicine*, 86(2), 1125–1136.  
<https://doi.org/10.1002/mrm.28768>
- 141 Dawson-Haggerty, M. (2023). *Trimesh* (Version 4.0.0). <https://github.com/mikedh/trimesh>
- 142 Fischl, B. (2012). FreeSurfer. *NeuroImage*, 62(2), 774–781. <https://doi.org/10.1016/j.neuroimage.2012.01.021>

- 147 Goebel, R. (2012). BrainVoyager — Past, present, future. *NeuroImage*, 62(2), 748–756.  
148 <https://doi.org/10.1016/j.neuroimage.2012.01.083>
- 149 Hall, J. E. (2015). *Guyton and Hall Textbook of Medical Physiology*. Elsevier Health Sciences.  
150 ISBN: 978-1-4557-7005-2
- 151 Huntenburg, J. M., Steele, C. J., & Bazin, P.-L. (2018). Nighres: Processing tools for high-  
152 resolution neuroimaging. *GigaScience*, 7(7), giy082. <https://doi.org/10.1093/gigascience/giy082>
- 153 Huntenburg, J., Wagstyl, K., Steele, C., Funck, T., Bethlehem, R., Fouquet, O., Larrat, B.,  
154 Borrell, V., & Bazin, P.-L. (2017). Laminar Python: Tools for cortical depth-resolved  
155 analysis of high-resolution brain imaging data in Python. *Research Ideas and Outcomes*, 3,  
156 e12346. <https://doi.org/10.3897/rio.3.e12346>
- 157 Ishikawa, M., Inoue, T., Kozawa, E., Okada, H., & Kobayashi, N. (2022). Framework for  
158 estimating renal function using magnetic resonance imaging. *Journal of Medical Imaging*,  
159 9(2), 024501. <https://doi.org/10.1117/1.JMI.9.2.024501>
- 160 Jenkinson, M., Beckmann, C. F., Behrens, T. E. J., Woolrich, M. W., & Smith, S. M. (2012).  
161 FSL. *NeuroImage*, 62(2), 782–790. <https://doi.org/10.1016/j.neuroimage.2011.09.015>
- 162 Li, L.-P., Milani, B., Pruijm, M., Kohn, O., Sprague, S., Hack, B., & Prasad, P. (2020). Renal  
163 BOLD MRI in patients with chronic kidney disease: Comparison of the semi-automated  
164 twelve layer concentric objects (TLCO) and manual ROI methods. *Magnetic Resonance*  
165 *Materials in Physics, Biology and Medicine*, 33(1), 113–120. <https://doi.org/10.1007/s10334-019-00808-5>
- 166 Lote, C. J. (2012). *Principles of Renal Physiology*. Springer Science & Business Media.  
167 ISBN: 978-94-011-4086-7
- 168 Milani, B., Ansaloni, A., Sousa-Guimaraes, S., Vakilzadeh, N., Piskunowicz, M., Vogt, B.,  
169 Stuber, M., Burnier, M., & Pruijm, M. (2017). Reduction of cortical oxygenation in  
170 chronic kidney disease: Evidence obtained with a new analysis method of blood oxygenation  
171 level-dependent magnetic resonance imaging. *Nephrology Dialysis Transplantation*, 32(12),  
172 2097–2105. <https://doi.org/10.1093/ndt/gfw362>
- 173 Piskunowicz, M., Hofmann, L., Zuercher, E., Bassi, I., Milani, B., Stuber, M., Narkiewicz, K.,  
174 Vogt, B., Burnier, M., & Pruijm, M. (2015). A new technique with high reproducibility  
175 to estimate renal oxygenation using BOLD-MRI in chronic kidney disease. *Magnetic*  
176 *Resonance Imaging*, 33(3), 253–261. <https://doi.org/10.1016/j.mri.2014.12.002>
- 177 Stevens, L. A., Coresh, J., Greene, T., & Levey, A. S. (2006). Assessing Kidney Function —  
178 Measured and Estimated Glomerular Filtration Rate. *New England Journal of Medicine*,  
179 354(23), 2473–2483. <https://doi.org/10.1056/NEJMra054415>
- 180 Yamashita, S. R., Atzingen, A. C. von, Iared, W., Bezerra, A. S. de A., Ammirati, A. L.,  
181 Canziani, M. E. F., & D'Ippolito, G. (2015). Value of renal cortical thickness as a predictor  
182 of renal function impairment in chronic renal disease patients. *Radiologia Brasileira*, 48(1),  
183 12. <https://doi.org/10.1590/0100-3984.2014.0008>
- 184
- 185